

## DESIGN CONSIDERATIONS AND ANALYSIS OF IN-WHEEL PERMANENT MAGNET SYNCHRONOUS MOTORS FOR ELECTRIC VEHICLE APPLICATIONS USING FEM

**Yannis L. Karnavas, Ioannis D. Chasiotis, Stefanos K. Amoutzidis**

Electrical Machines Laboratory, Dept. of Electrical & Computer Engineering,  
Democritus University of Thrace, Xanthi, Hellas (GR), karnavas@ee.duth.gr

***Abstract*** – The paper presents design considerations of permanent magnet synchronous motors (PMSM) with concentrated windings and outer rotor topology for a light in-wheel electric vehicle (EV) application. A wide poles/slots range considered initially as a search space and machines with 48-poles/54-slots and 60-poles/63-slots were finally adopted. Finite element analysis (FEA) is employed in order to determine the performance of each motor. Systematic optimization on slots, permanent magnet's (PM) height and pole-arc to pole-pitch ratio was conducted, and relevant results are presented. It is shown that the maximum torque capability, the low torque ripple, the low cogging torque and low weight of the particular machines are well fitted to the specific EV application.

### **1. Introduction**

In-wheel motors are traction motors which actually change rotary motion to linear motion. Their attachment to the wheel is not implemented through gearing; instead they are part of the wheel itself [1]. This fact limits these direct-drive motors to a size that will fit inside the wheel, while at the same time performance requirements should be preserved. Recent literature findings reveal that PMSMs exhibit high torque-to-inertia ratios as well as efficiency thus are suitable candidates for this kind of EV traction. Ref. [2] for example, has focused on a surface PM type axial gap structure that can achieve a high torque density and a short motor length in the axial direction. The designed motor structure with ferrite PMs replacing the rare earth PMs was introduced and relevant 3-D finite element analysis results shown. In [3], an investigation of the potential advantages of PMSM compared to flux-switching machines, particularly for the applications of EV traction has been conducted. Fault tolerant and multi-phase motors studies have also been found in literature. Ref. [4] focused on achieving a high torque density and the ability to sustain an adequate level of performance following a failure, while [5] and [6], investigated fault-tolerant modular in-wheel PMSMs for EV wheel driven applications and also applicable slot/pole combinations for five-phase and six-phase machines respectively were recommended. Self-deceleration issues in high torque/low-speed motors have also been investigated recently [7]. From an industrial perspective, considerable research effort has been put into studying the behavior of appropriate PMSMs, and it has been found that motors with concentrated windings are advantageous than those with distributed ones [8], [9]. That research effort though, was conducted w.r.t. inner-rotor topologies mainly, so outer-rotor ones –with or without hybrid excitation- have to be studied more [10]. Despite the fact that the outer rotor designs may suffer from cooling issues (since they exhibit much less cooling surface), there are many advantages which make them suitable candidates [11]. Some of these advantages are: a) they have significantly higher split ratio (the rotor outer diameter/stator outer diameter), b) they require much lower flux density ratio for the maximum torque, c) for surface magnets the outer rotor design exhibit higher torque than the inner rotor, d) copper losses of outer rotor designs can be significantly lower than the inner rotor topology, e) inner rotor topologies are much heavier and more expensive, f) outer rotor require less magnet volume. In this context, this work aims to investigate, optimize, compare and propose suitable outer-rotor machines for a specific light EV application along with the relevant results.

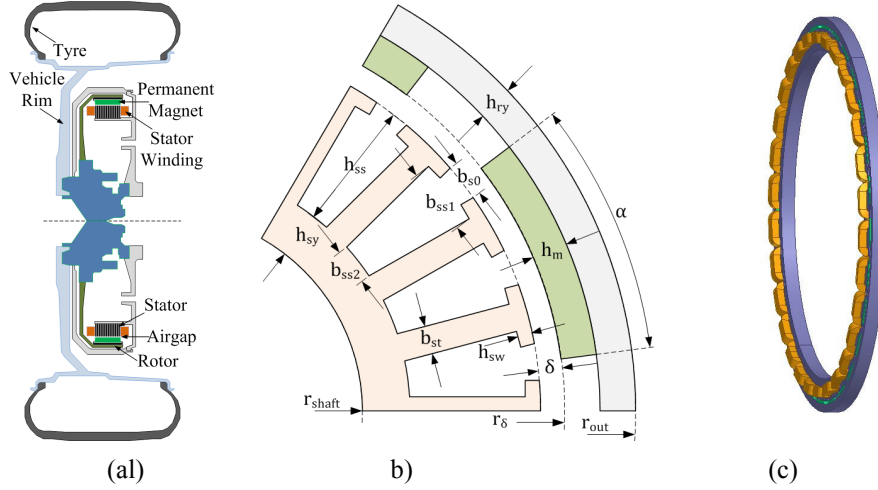


Fig. 1. Problem schematic representations, a) Cross section of an in-wheel motor assembly, b) Geometry topology of an outer-rotor PMSM used here, c) General 3D view of motor type under consideration.

## 2. In-Wheel Outer Rotor PMSM Analytical Model Design Calculations

Fig. 1(a) depicts the “housing” requirements of an in-wheel motor. Components such as mechanical brakes and the suspension which may be placed also inside the wheel have an effect on the heat transmission which, in this case is neglected. However this omission of the brake modeling is of particular importance due to the heat dissipation during operation. Fig. 1(b) shows the PMSM’s outer rotor topology, where all the parameters shown have to be optimized while satisfying certain constraints. For the sake of space, these parameters will be explained, among others, as text follows. Finally, Fig. 1(c) depicts a generic 3D view of the motors under consideration. In this paragraph, several analytical formulas are presented along with the relevant quantities involved in this motor type design. The reader can refer to [12]-[14] for more details.

**a) Winding Configuration:** For a three phase machine, the number of slots per pole and phase  $q$  is given by  $q=Q/3p$ , where  $Q$  is the total number of slots and  $p$  is the number of poles. If this value is less than unity, the winding is referred to as a concentrated. Concentrated windings can be single-layered, with alternate wound teeth, i.e., one coil side per slot, or double-layered, with all the teeth wound and two coils sharing one slot. Double-layered concentrated windings produce less losses and torque ripple whereas single-layered concentrated windings provide a high fault tolerance since the different phases are isolated. This study employs double layer concentrated windings.

**b) Speed:** In the steady state, the mechanical speed of the machine in rpm is given by  $n=120f/p$  where  $f$  is the input frequency and  $p$  the number of poles.

**c) Torque:** The torque equation for a general rotor topology can be expressed as

$$T_e = \frac{4}{\pi} S_l B_\delta f_{wl} (D - \delta)^2 L \sin \beta \quad (1)$$

where  $S_l$  is the peak fundamental current loading,  $B$  is the peak fundamental open-circuit air gap flux density,  $f_{wl}$  is the fundamental winding factor,  $D$  is the inner stator diameter,  $\delta$  is the air gap length,  $L$  the active length and  $\beta$  the angle between the d-axis and the current vector.

**d) Losses:** The losses in the machine windings are pure resistive and can be expressed as

$$P_{Cu} = 3R_s i^2 \quad (2)$$

where  $R_s$  is the stator resistance and  $i$  is the rms phase current. The iron losses consist of hysteresis and Joule losses. Assuming a purely sinusoidal flux density variation, the hysteresis losses and eddy current losses per mass unit can be expressed as

$$P_{hyst} = k_{hyst} \omega B_m^\beta \quad P_{eddy} = k_{eddy} \omega^2 B_m^2 \quad (3)$$

where  $k_{hyst}$  and  $k_{eddy}$  are the hysteresis and eddy current constants for steel,  $\omega$  is the electrical angular speed,  $B$  is the peak magnetic flux density and  $\beta$  is the Steinmetz constant for steel. However, in the analytical model, the fundamental copper losses based on Eq.(2) can be expressed as,

$$P_{cu} = \frac{3}{2} R_s (i_d^2 + i_q^2) \quad (4)$$

where the factor  $i_d^2 + i_q^2$  is the peak fundamental phase current squared. To account for the motor iron losses, both hysteresis and eddy current losses are considered here. The losses are calculated separately in the stator yoke and teeth with Eqs.(5):

$$P_{sy} = (k_{hyst} \omega B_{st}^\beta + k_{eddy} \omega^2 B_{sy}^2) m_{sy} \quad P_{st} = \left( k_{hyst} \omega B_{st}^\beta + 12q \frac{b_{ss} + b_{st}}{\pi^2 b_{st}} k_{eddy} \omega^2 B_{sy}^2 \right) m_{st} \quad (5)$$

where  $m_{sy}$  and  $m_{st}$  are the stator yoke and stator teeth weights respectively.

**e) Geometry:** The motor geometry and its parameters are represented in Fig.1(b). The relations between the different geometrical parameters can be found as

$$\begin{aligned} r_\delta &= r_{out} - h_{ry} - h_m - \delta & b_{ss1} &= \frac{2\pi(r_\delta - h_{sw})}{3pq} - b_{st} \\ h_{sy} &= r_\delta - h_{ss} - r_{in} & b_{ss2} &= \frac{2\pi(r_\delta - h_{ss})}{3pq} - b_{st} \\ \alpha &= 2\alpha_{elec} / p \end{aligned} \quad (6)$$

where  $p$  is the number of poles,  $q$  is the number of slots per pole and phase and  $\alpha_{elec}$  represents the electrical angle covered by the magnets. The width of a stator tooth  $b_{st}$  is constant along the whole tooth section. For the geometrical calculations,  $b_{ss1}$ ,  $b_{ss2}$  and  $b_{st}$  are approximated as straight lines instead of arcs of circumference.

**f) Current and Torque Dynamics:** The equations that describe the motor behavior are presented now. The peak fundamental phase voltage  $E$  of a PM motor is produced by the magnets according to the expression  $E = \omega \psi_m$  where  $\psi_m$  is the permanent-magnet flux linkage and  $\omega$  is the electrical synchronous angular speed. In the steady state and if neglecting harmonics, the voltage d- and q-components of the motor can be expressed as

$$u_d = R_s i_d - \omega \psi_q = R_s i_d - \omega L_q i_q \quad u_q = R_s i_q - \omega \psi_d = R_s i_q - \omega (\psi_m + L_d i_d) \quad (7)$$

The torque is given by Eq.(6) (a complete deduction of it can be found in, e.g., [14]).

$$T_e = \frac{3}{2} \frac{p}{2} [\psi_m i_q - (L_q - L_d) i_q i_d] \quad (8)$$

In this case, since the magnets are surface mounted, the air paths in d- and q-directions have the same length which means that  $L_d = L_q = L_s$ . Thus, the torque expression can be simplified to

$$T_e = (3/4) p \psi_m i_q \quad (9)$$

**g) Other Relations:** The fundamental winding factor for a concentrated winding 3 phase motor with  $q$  slots per pole and phase is given by

$$f_{w1} = \frac{\sin(h\sigma/2)}{z \sin(h/2\sigma z)} \cos\left(\frac{1}{2} h \pi \left(1 - \frac{1}{3q}\right)\right) \quad (10)$$

where  $h$  is the winding space harmonic order,  $\sigma$  is the phase spread angle and  $z$  equals to  $Q/\text{gcd}(Q, 3p)$  (gcd: greatest common divider). Also, neglecting magnetic saturation, the expression for the synchronous inductance  $L_s$  of a surface mounted inner rotor permanent magnet motor is reported in [14] and it can be rewritten for an outer rotor motor as

$$L_s = \frac{3}{\pi} \frac{2\mu_0 (r_{out} - h_{ry} - h_m - c_f \delta) L}{c_f \delta + h_m / \mu} (f_{w1} q n_s)^2 \quad (11)$$

where  $\mu_0$  and  $\mu_r$  are the relative permeability of the vacuum and magnets respectively,  $r_{out}$  is the outer radius of the motor,  $h_{ry}$  is the rotor yoke height,  $h_m$  is the magnet height,  $\delta$  is the air gap length,  $L$  is the active length of the motor,  $f_{w1}$  is the fundamental winding factor,  $n_s$  is the number of turns per slot and  $c_f$  is the Carter factor which accounts for the equivalent air gap including the effect of the stator slots.

**h) Current operating points:** The motor torque capability is limited by the maximum current and by the dc-link voltage supplied by the EV's battery (Fig. 2). These limitations can be summarized:

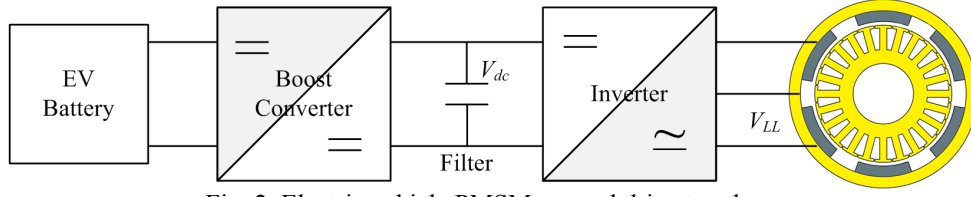


Fig. 2. Electric vehicle PMSM general drive topology.

$$\sqrt{i_d^2 + i_q^2} \leq i_{\max} \quad \sqrt{u_d^2 + u_q^2} \leq u_{\max} = V_{dc} / \sqrt{3} \quad (12)$$

If the resistive voltage drop is neglected, Eqs.(7) can be rewritten as

$$u_d = -\omega L_s i_q \quad u_q = \omega(\psi_m + L_s i_d) \quad (13)$$

By substituting Eqs.(13) in Eqs.(12), the following relation is obtained

$$\left(i_d + \frac{\psi_m}{L_s}\right)^2 + i_q^2 \leq \left(\frac{u_{\max}}{\omega L_s}\right)^2 \quad (14)$$

which in the dq-current plane describes a circle of radius  $u_{\max}/\omega L_s$  and centered in  $(-\psi_m/L_s, 0)$  in which the voltage restriction is fulfilled. Together with the maximum current restriction, this describes the possible operation points of the motor for all speeds.

At this point, an important factor which plays a key role is the motor's slot/pole number combination. Based on a methodology developed in previous work [15], the 48/54 and 60/63 outer rotor configurations were finally chosen. That methodology actually performed an overall motor's structure (Fig.1(b)) optimization procedure based in three optimization methods (fmincon, genetic algorithms and pattern search). In addition the pole-arc to pole-pitch ratio and PM's height were two of the search variables. The optimization was performed until certain cost functions were minimized regarding the motors' copper losses, PM's weight and overall machine weight.

### 3. Analysis Methodology and Results

Continuing to optimization based on the analytical model, for the computation of the motors' performance quantities, time-stepping FEM software was used which solves the well-known time-dependent magnetic motion equation,

$$\nabla \times \nu \nabla \times A = J_s - \sigma \frac{\partial A}{\partial t} + \sigma \nabla V + \nabla \times H_c \quad (15)$$

Also, due to the short axial length of the motors in consideration, there is a considerable axial end effect. Thus, 3D analysis should be performed to account for that effect and confirm the results. The initial rotor position was set in order to match the direction of the magnetic field created by the stator currents in that moment. Thus, an initial rotor angle is introduced for each motor. To account for eddy currents in the magnets, which are typically a 3D issue in a 2D study, the total eddy currents in each magnet have to be set to zero by introducing a FEM conductor in them and connecting it to ground. This will assure that the amount of upward and downward magnet currents is the same and, thus, the approximate eddy currents are considered. Regarding the computational mesh, it is known that it has to be small enough to avoid having big numerical errors. Although, in general, an element size of 0.5mm may be adequate, an adaptive mesh is set in all models which subdivide those elements which largely affect the results into smaller ones. In this way, the stator teeth's outer borders which are mainly subject to saturation are automatically reset to a smaller element size. Table 1 and Table 2 show the specific EV application requirements and problem constraints respectively, while Table 3 the materials' data finally chosen. With respect to Fig. 1(b), the analytical problem description and the procedure described above, Table 4 and Table 5, show the overall obtained results. It can be seen that all the constraints were met satisfactorily while the efficiency for both motors proposed ("Motor 1" and "Motor 2") found high enough. Moreover, the machines weight was found less than the 17kg limitation. Finally, Fig.3 and Fig.5 depicts the magnetic field distributions respectively, while Fig.4 and Fig.6 depict several plots of quantities of importance along with their harmonics analyses. Of special interest is also the cogging torque and

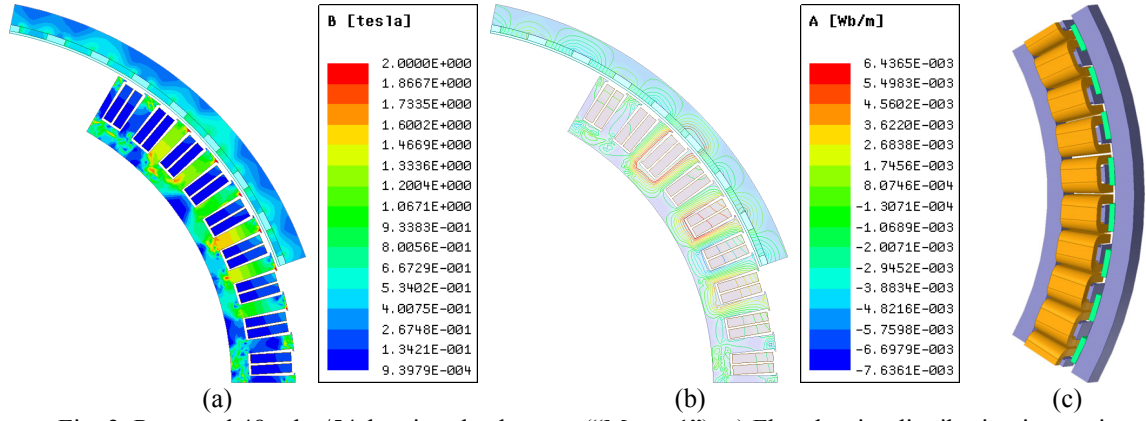


Fig. 3. Proposed 48poles/54slots in-wheel motor (“Motor 1”): a) Flux density distribution in running condition, b) Flux lines distribution, c) Designed 3D cut-out view (1/6<sup>th</sup> part).

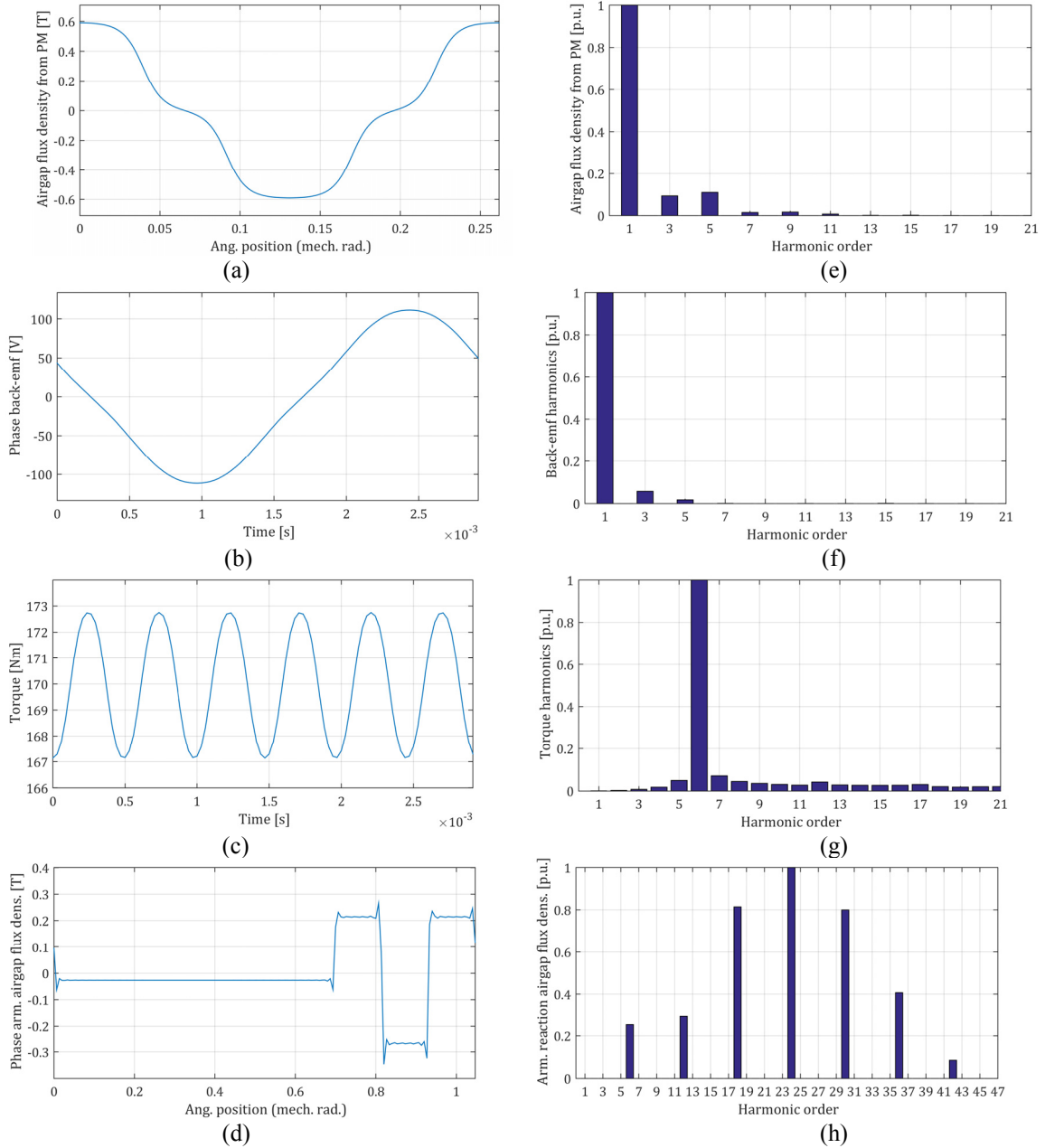


Fig. 4. Results of the proposed 48pole/54slots motor (“Motor 1”), (a) PM’s airgap flux density, (b) phase back-emf, (c) torque, (d) armature reaction airgap flux density, (e), (f), (g), (h) corresponding harmonics.

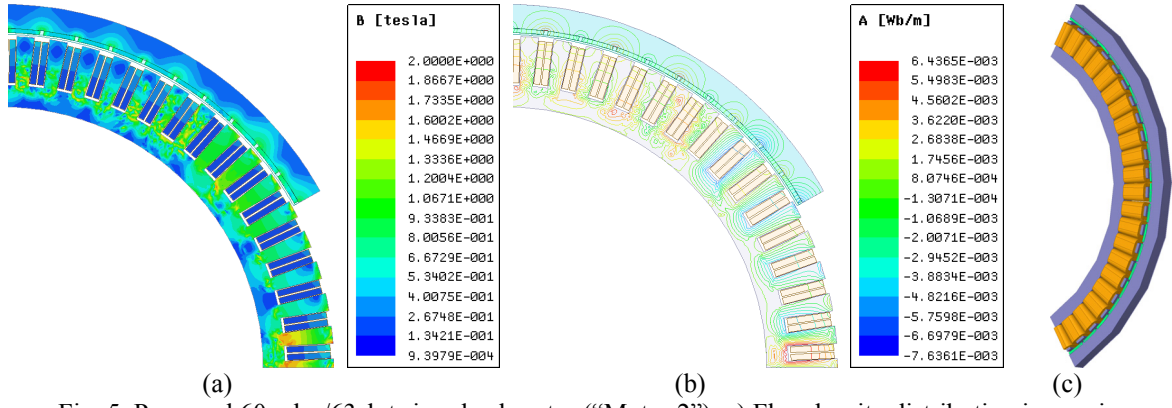


Fig. 5. Proposed 60poles/63slots in-wheel motor ("Motor 2"): a) Flux density distribution in running condition, b) Flux lines distribution, c) Designed 3D cut-out view (1/6<sup>th</sup> part).

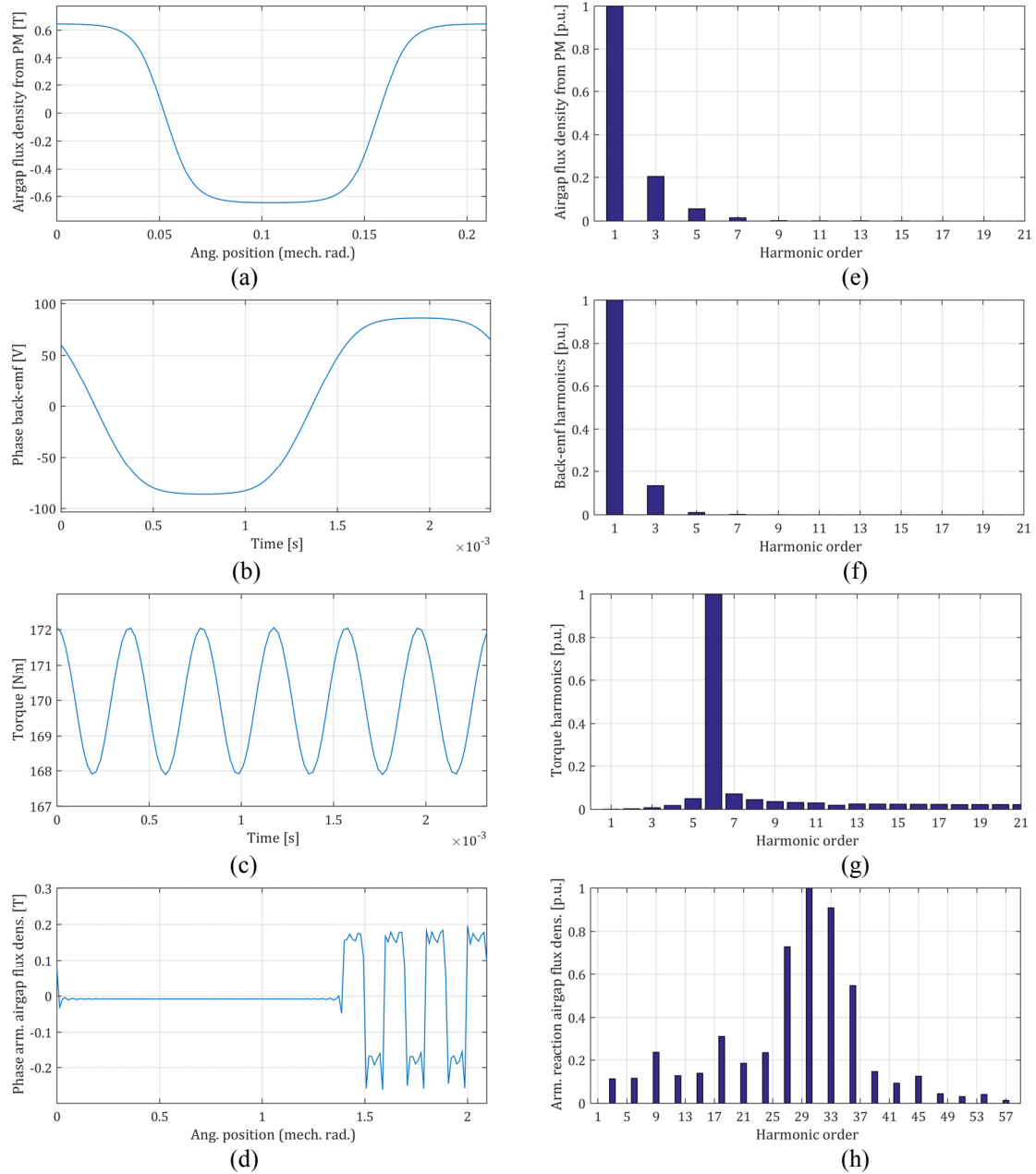


Fig. 6. Results of the proposed 60pole/63slots motor ("Motor 2"), (a) PM's airgap flux density, (b) phase back-emf, (c) torque, (d) armature reaction airgap flux density, (e), (f), (g), (h) corresponding harmonics.

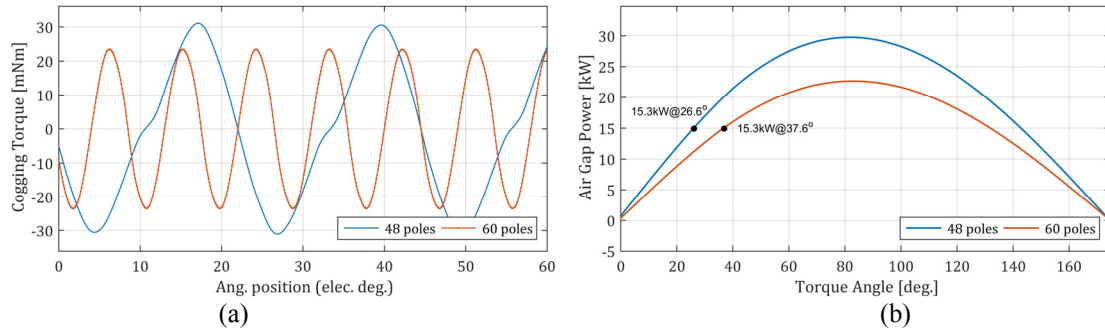


Fig. 7. Proposed in-wheel motors' performance quantities: a) Cogging torque, b) Developed airgap power.

Table 1. EV in-Wheel Motor Requirements.

Quantity	Symbol	Value	Unit
Output power	$P_{out}$	15300	[W]
Output torque	$T_{out}$	170	[Nm]
Number of poles	$p$	$20 \leq p \leq 80$	-
Synchronous speed	$n_s$	850	[rpm]
DC link voltage	$V_{dc}$	400	[V]
Inverter's modul. ratio	$m_a$	0.69	-
Slots per pole/phase	$q$	$0.1 \leq q < 1$	-
Conductors/slot	$n_c$	$1 \leq n_c \leq 60$	-
Active length	$L$	30	[mm]
Outer radius	$r_{out}$	216	[mm]

Table 2. Design Problem Constraints.

Description	Symbol	Constraint
Sator yoke flux density	$B_{sy}$	$\leq 1.8$ T
Sator teeth flux density	$B_{st}$	$\leq 1.8$ T
Rotor yoke flux density	$B_{ry}$	$\leq 1.8$ T
Airgap flux density	$B_{\delta}$	$\leq 1.1$ T
Airgap length	$\delta$	$\geq 1$ mm $\leq 3$ mm
Sator yoke height	$h_{sy}$	$\geq h_{ss}/3$
Rotor yoke height	$h_{ry}$	$\geq 8$ mm
Slot base width	$b_{ss2}$	$\geq (0.15 h_{ss})$ mm $\leq (0.5 h_{ss})$ mm
Sator teeth width	$b_{s0}$	$\geq 2.0$ mm
Sator teeth width	$b_{st}$	$\geq 2.5$ mm
Magnet height	$h_m$	$\geq 2.5$ mm $\leq 10$ mm
Copper Losses	$P_{Cu}$	$\leq 900$ W
Magnet weight	$M_m$	$\leq 1.0$ kg
Machine weight	$M_w$	$\leq 17$ kg

Table 3. Motors' Material Data.

Constant	Symbol	Value
Magnet: Remanent flux dens.	$B_r$	1.23 T
NdFe35 Rel. permeability	$\mu_r$	1.09
Magnet density	$\rho_m$	7400 kg/m <sup>3</sup>
Steel: Rel. permeability	$\mu_r$	4000
M19_24G Conductivity	$\sigma_s$	$1.96 \times 10^7$ S/m
Steel density	$\rho_s$	7650 kg/m <sup>3</sup>
Rel. permeability	$\mu_r$	$9.99 \times 10^{-1}$
Winding Conductivity	$\sigma_{Cu}$	$5.8 \times 10^7$ S/m
Copper density	$\rho_{Cu}$	8900 kg/m <sup>3</sup>

Table 4. Results of Design Variables\*.

Quantity	Symbol	Motor 1	Motor 2
No. of poles	$p$	48	60
No. of slots	$Q_s$	54	63
Motor shaft radius	$r_{shaft}$	162.47	155
Motor outer radius	$r_{out}$	216	216
Air gap radius	$r_{\delta}$	200.87	199.12
Air gap length	$\delta$	2.5	2.12
Slot opening width	$b_{s0}$	12.05	9.0
Slot top width	$b_{ss1}$	15.0	9.01
Slot base width	$b_{ss2}$	12.46	9.02
Sator teeth width	$b_{st}$	7.96	10.53
Sator tooth tip height	$h_{sw}$	1.0	1.0
Sator slot height	$h_{ss}$	25.92	29.0
Sator yoke height	$h_{sy}$	9.98	13.0
Rotor yoke height	$h_{ry}$	11.63	14.37
Magnet height	$h_m$	3.5	2.5
Pole arc/pole pitch ratio	$\alpha$	0.6	0.9
Slot fill factor	$s_f$	0.6	0.6
No. of conductors/slot	$n_c$	16	14
No. of wires/conductor	$n_w$	1	1
Wire diameter	$d_w$	3.665	3.264
No. of layers	$n_l$	2	2
Winding factor	$k_w$	0.945	0.953

\*(all dimensions in mm).

Table 5. Electromechanical Quantities Results.

Quantity	Symbol	Motor 1	Motor 2
Efficiency (%)	$\eta$	94.97	95.41
Line current (A)	$I$	92.41	70.44
Current density (A/mm <sup>2</sup> )	$J_c$	6.57	6.81
Copper losses (W)	$P_{Cu}$	722.06	604.61
Core losses (W)	$P_{Core}$	87.75	132.44
Magnet weight (gr)	$M_m$	593.45	628.85
Machine weight (kg)	$M_w$	12.49	14.77
Cogging torque (Nm)	$T_{cog}$	0.031	0.023
Torque ripple (%)	$T_{rip}$	3.3	2.4
Torque angle (deg)	$T_{ang}$	26.62	37.61
Fund. ind. voltage (V)	$emf$	153.89	175.87
Nom. frequency (Hz)	$f$	340	425



the airgap's developed power, whose plots are shown comparatively for the two motors in Fig.7. It is also seen that "Motor 1" would be a better choice if weight is crucial, while "Motor 2" prevails in case that battery capacity and subsequently the EV's kilometer range with a single charge is much more important.

#### **4. Conclusions**

In this paper, design considerations for the design of in-wheel PMSM for light EV applications were presented. Having specific motor requirements as well as problem constraints for a complete set of electromechanical and magnetic quantities, a wide search space for possible pole/slots combinations was examined first and two outer rotor PM machines were proposed, optimized individually and compared in terms of many aspects such as PM's airgap flux density, phase back-emf, torque, armature reaction airgap flux density, cogging torque and airgap developed power. The analyses for the 48/54 and 60/63 machines were primarily based on an analytical model approach and thereafter FEM applied and detailed results obtained and presented. It was shown that both designs succeeded to satisfy the relevant constraints and may be suitable candidates for the specific in-wheel EV application. It should be noted however that for fair comparisons, other important design considerations, such as demagnetization and thermal analyses, are required and there is an ongoing effort in order to report further relevant results in a future paper.

#### **5. References**

- [01] Watts, A., Vallance, A., Whitehead, A., Hilton, C. et al., "The Technology and Economics of In-Wheel Motors," *SAE Int. J. Passeng. Cars - Electron. Electr. Syst.*, vol. 3, no. 2, 2010, pp. 37-57.
- [02] K. Sone, M. Takemoto, S. Ogasawara, K. Takezaki, H. Akiyama, "A ferrite PM in-wheel motor without rare earth materials for electric city commuters", *IEEE Transactions on Magnetics*, vol. 48, no. 11, Nov. 2012, pp. 2961-2964.
- [03] Y. Tang, E. Motoasca, J. Paulides, E. Lomonova, "Comparison of flux switching machines and permanent magnet synchronous machines in an in-wheel traction application", *COMPEL - The international journal for computation and mathematics in electrical and electronic engineering*, vol. 32, no. 1, pp. 153-165.
- [04] I. Chukwuma, M. Barrie, B. Simon, B. Gerard, A. Glynn, K. Dragica, "Fault-tolerant in-wheel motor topologies for high-performance electric vehicles", *IEEE Transactions on Industry Applications*, vol. 49, no. 3, May 2013, pp. 1249-1257.
- [05] Z. Ping, S. Yi, Z. Jing, T. Chengde, T.A. Lipo, W. Aimeng, "Investigation of a novel five-phase modular permanent magnet in-wheel motor", *IEEE Transactions on Magnetics*, vol. 47, no. 10, Oct. 2011, pp. 4084-4087.
- [06] Z. Ping, W. Fan, L. Yu, S. Yi, Y. Bin, "Investigation of a novel 24-slot/14-pole six-phase fault-tolerant modular permanent magnet in-wheel motor for electric vehicles", *Energies*, 2013, pp. 4980-5002.
- [07] F. Ying, Z. Li, H. Jin, H. Xuedong, "Design, analysis, and sensorless control of a self-decelerating permanent-magnet in-wheel motor", *IEEE Transactions on Industrial Electronics*, vol. 61, no. 10, Oct. 2014, pp. 5788-5797.
- [08] J. Cros, P. Viarouge, "Synthesis of High Performance PM Motors With Concentrated Windings", *IEEE Trans. on Energy Conversion*, vol. 17, no. 2, June 2002, pp. 248-253.
- [09] Y. Y. Choea, S. Y. Oha, S. H. Hamb, I. S. Janga, S. Y. Choa, "Comparison of Concentrated and Distributed Winding in an IPMSM for Vehicle Traction", *Energy Procedia*, vol. 14, 2012, pp. 1368-1373.
- [10] M. Ahmad, F. Sulaiman, Z. Haron, H. Kosaka, "Impact of rotor pole number on the characteristics of outer-rotor hybrid excitation flux switching motor for in-wheel drive EV", *Procedia Technology*, vol. 11, 2013, pp. 593-601.
- [11] W.Q. Chu, Z.Q. Zhu, "Optimal split ratio and torque comparison of surface permanent magnet machines having inner or outer rotor", in *Proc. of 6<sup>th</sup> Intl. Conf. on Power Electronics, Machine and Drives (PEMD)*, Bristol, March 27-29, 2012, pp. 1-6.
- [12] F. Meier, "Permanent magnet synchronous machines with non overlapping concentrated windings for low-speed direct-drive applications", PhD Thesis, Royal Institute of Technology, KTH, Stockholm, Sweden, 2008.
- [13] D. Hanselman, *Brushless Permanent Magnet Motor Design*, Orono, USA: The Writers' Collect., 2003.
- [14] C. Sadarangani, "Electrical Machines. Design and Analysis of Induction and Permanent Magnet Motors", Stockholm, Sweden, Royal Inst. Technol., 2006.
- [15] Y. L. Karnavas, C. D. Korkas, "Optimization Methods Evaluation for the Design of Radial Flux Surface PMSM", in *Proc. of 21<sup>st</sup> Intl. Conf. on Electrical Machines (ICEM)*, Berlin, 2-5 Sept. 2014, pp. 1348-1355.